Laser Fragmentation of Gall Stone

A Thesis Submitted
In partial Fulfillment of the Requirements
For the Degree of

Master in Technology

by

Shiv Govind Singh

to the

Laser Technology Programme
Indian Institute of Technology Kanpur

September, 1998

Certificate

It is certified that the work contained in the thesis entitled "***Laser Fragmentation of Gall Stone***" by ***Shiv Govind Singh*** Roll No. ***9611608*** has been carried out under my supervision and that this work has not been submitted elsewhere for a degree.

RK Thareja

(R. K. Thareja)

Professor

Department of Physics &

Laser Technology Program

I. I. T. Kanpur.

September, 1998.

Acknowledgements

I express my sincere gratitude to Prof. R. K. Thareja for giving me the opportunity to work in a kind of growing field. I have gained a lot during my project under his able guidance.

I would like to thank Mr. Ashutosh Misra and Mr. Anirban Mitra for their valuable co-operation during the experiments and in compiling the thesis.

I thank all my labmates Amit Neogi, V. Narayanan, Ashwini K. Sharma and Tripti Srivastava.

A word of thank to Dr. (Mrs.) Sukarma Thareja for her moral support during my work.

I acknowledge the help of Dr. Asima Pradhan for giving me He-Ne laser and Dr. Asha Agarwal for providing me different types of Gallstones and information regarding them.

I take this opportunity to thank staff members of CELT Workshop and CELT office for their help during the course of my work.

I am thankful to my friends D.K., Manish, Brijesh, Alok, Rajan, Rajesh, Bhuvanesh, Nirmal, Indranil, Salil, Pankaj, Daniel, Kenge, Biju, J.P., Amit, Narsimhan, Gaurav, Vivek, Nahbhatti, Aniraban and others who made my stay memorable at IIT Kanpur.

Last but not the least I am also grateful to my parents and brothers and sisters for their constant moral support.

Shiv Govind Singh

TABLE OF CONTENTS

LIST OF FIGURES

LIST OF SYMBOLS

c	Velocity of light in medium
c_0	Velocity of light in vacuum
f	focal length of lens
G	Constant which depends upon Photo Detector sensitivity
K	Gain constant
l	Interaction length
L	Distance from the interaction region in the cell to photodiode
$n(r,t)$	Change in refractive index
n_0	Normal refractive index
P	Pressure
S_o	Gain constant when beam deflection is zero
W	Beam waist
ρ	Density
ρ_s	Reference density of gas at 0^0 C and 760 mm pressure
τ	Time interval
$d\xi$	Length traversed by light ray along the direction r
ϕ	Total angular deflection of probe beam
ω_e	Beam radius
λ	Wavelength of laser light

Name of Student	: Shiv Govind Singh
Roll No.	: 9611608
Department	: Laser Technology Program
Thesis Title	: Laser Fragmentation of Gall Stone
Name of Thesis Supervisor	: Professor R. K. Thareja
Month and year of Thesis submission	: September, 1998

Abstract

Study of laser interaction with biological materials in liquid environment is becoming an important phenomenon because of its wide use in medical applications like laser lithotrispy, corneal surgery, angioplasty etc. Photoacoustic Beam Deflection is a useful technique for the detection of transient pressure pulses generated in water during the interaction of laser with other materials. In this study the measurements of absolute pressure at different laser fluences is presented. Laser ablation thresholds for different materials like Gallstone and aluminum are also measured. Study of laser interaction with water has also been done. It is observed that FWHM of the pressure pulses gradually increase with increasing laser fluences. As the laser fluence is increased above the ablation threshold, the signal of the pressure wave reduces due to the scattering of the ablated materials. Variations of the focused point of the pump laser at different distances from the target surface show first increment and then gradually decrement of the pressure pulses.

CHAPTER I

Introduction

During last few years clinical methods employing lasers to ablate biological tissues has grown immensely. Though the research in this field (both theoretically and experimentally) is under progress, still the basic mechanism of ablation processes in biological systems are not completely understood.

In order to have a better insight of the ablation process in biological samples, the ablation process is divided in to three different heads, namely: photochemical, photomechanical and photothermal. In the photochemical process, the absorption of laser photons leads directly to the dissociation of molecular bonds, whereas in, both the other two processes it is the laser induced stress, which ruptures the biological units.[1] For ablation using short pulsed lasers, there is an evidence that photomechanical effect play a vital role in ablation processes.[2,3]

For a photomechanical process to hold, the laser-induced stress should exceed the strength of the material being irradiated. As soon as the laser pulse enters the sample, scattering and absorption takes place, thus creating non- uniform temperature and stress distribution within the sample. It is now well established that the biological samples e.g. tissues are weaker in tension and hence it has been conjugated that the tensile acoustic traveling wave causes the material to rupture. This type of photomechanical process is also termed as laser induced spallation (LIS)[4,5]. It has been shown that LIS play an important role in ablation of metals with low Z. However, the biological samples, exhibit a different behavior since the spallation occurs at and near the surface of the target sample, whereas the amplitude of the acoustic tensile waves become significant an order of magnitude deeper into the target. This process of ablation accounts for significant increase in the ablation threshold as the pulse duration of the laser increases or if the target sample is placed in water liquid environment instead of air, in contrast to the existing experimental works.[2] In photochemical process, laser energy gets deposited in the tissue and the tissue is vaporized. This process occurs only for irradiation with long pulse or continuos wave lasers.

The inconsistency between prediction of 1D spallation model and experimental observation is due to some important features not considered in the model. In addition to axial stress considered in 1D spallation model there are three other important stress (radial, shear, and circumferal) which must be considered in 3D geometry. The acoustic components of these are transient and propagate with the speed of sound, and therefore, remain in region for short times. Unlike in 1D case, however, in the 3D case these are also long-lived quasi-steady state thermoelastic components of the stress, which exponentially dissipate by thermal diffusion. Since these quasi-steady state stresses persist for many orders of magnitudes lower in times than the transient stresses, they can play more significant role in the ablation process. When these feature are taken into account the inconsistencies in the photomechanical model of ablation can be removed.

Human tissue can be divided into two classes based on its response to laser ablations.

1. Soft tissue, which includes muscle, fat, skin, blood vessels and the various internal organs.
2. Hard tissue, which includes bone, teeth and calcified plaque, which is often the result of the disease process. Soft tissue consists of primarily of proteins, with a large amount of water and many trace constituents, such as electrolytes and complex organic molecules. Hard tissue consists of composite of material consisting of calcium-phosphate salt imbedded in soft tissue matrix.

It is apparently surprising that the low energy density deposited in tissues before ablation occurs persists over a wide range of wavelength and pulse widths as well as for different types of tissues. The reason may be the change in optical properties of the tissue during the laser ablation pulse, which enhance the absorption of light. Such a change in optical properties is highly variable with wavelength. The difference in the magnitude of energy density in the near ultraviolet, visible and infrared may be order of magnitude.

Hard tissue are calcified tissues of the body and composite material in which micro-crystallites of calcium salt are embedded in a soft connective tissue matrix .[6,7] The matrix provides tensile strength while dolt provides compressive strength. In compact bone the inorganic fractions are mostly made up of hydroxy appetite salts densely deposited in a highly organized collagen matrix with small precipitates of

residual water. Urinary calculi have no soft component, so do not constitute a composite substance. For this reason, they are very brittle and broken by ultra sound.

Ablation of hard tissue can be described in terms of inertial confinement model. Inertial confinement causes large pressure and pressure gradients. The soft components bond fails in tension and material is accelerated. The soft crystal remains intact, however the soft components rapidly expands and exerts a force on the salt granules through momentum transfer and viscous drag. At sufficiently high irradiance the salt granules become dislocated and are accelerated out of crater. Fig 1.1 is a schematic of this process the ablation of calcified tissue is studied at all wavelengths of irradiation above 10^6 w/cm^2. This is consistence with calculation which indicates that vapor velocities of few hundreds meter/sec. are needed to drag 1-10 μm hydroxy particles out of crater. This model is consistent with strobe photography experiment.

Laser have found increasing application in many aspects of medicine and are used in many surgical procedures. The cutting or vaporization of tissue or stone with infrared laser in air is essentially thermal in nature. However in liquid environment the ablation seems to be non thermal. In the short pulsed laser light interaction with liquid, an enhanced pressure production has always been observed[8]. The efficiency of coupling of laser light into pressure is of great interest in many techniques are used in medical area, such as laser cleaning of surface contamination,[9] laser tissue ablation, corneal sculpturing[10] and gall stone fragmentation[11]. It is also used for surface treatment of metal and nondestructive testing of material[12]. The enhancement of pressure in liquid[13] or at its interface with another medium has been attributed to plasma formation, bubble cavitation and rapid evaporation. Plasma formation occurs due to ablation or optical breakdown of materials by high intensity laser irradiation.

Several in vitro and vivo studies have been made of gallstone fragmentation using Q-switched Nd:YAG or flash lamp pumped dye laser[14-19]. Gallstone has been successfully fragmented in experiments on animal and human. In the earlier work on laser lithotripsy there have been studies of statistics of gallstone fragmentation,[14-15] thermal damage to surrounding tissue,[14,20] time resolved optical emission spectroscopy[17,18] and determination of effect of liquid environment on fragmentation efficiency.[19] It has been previously reported that pressure ranging from few atmospheres up to hundreds of bar is generated upon laser interaction with absorbing liquid to transparent liquid near the absorbing solid boundary. Reported pressure

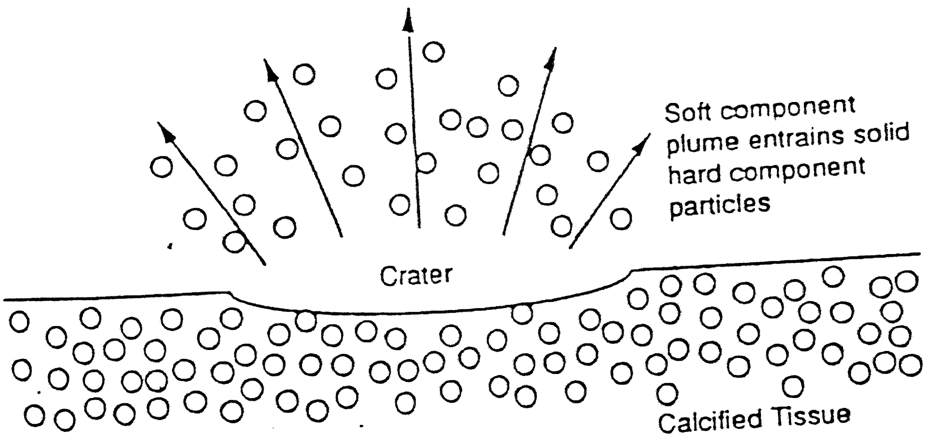

Fig. 1.1 Idealized schematic of two component concept of calcified tissue ablation.

value however depends upon laser intensity optical properties of liquid and/or absorbing solid, characteristics of pressure wave and the detector geometry. Hence in practice more universal parameter, namely, the conversion efficiency[19] from the optical energy delivered by laser pulse into the acoustic energy is usually utilized. The parameter ranges from 10^4 in the case of thermoelastic expansion[21] in the case of optical breakdown. It has been shown that the optical breakdown[22] or surface ablation and subsequent plasma formation are most efficient mechanisms for pressure generation[23]. However these are not desirable in many technical applications due to their destructive nature. The explosive vaporization of liquid on the other hand can generate pressure efficiently without infecting pressure damage on the sample. It has been shown that additional evaporation of liquid causes the peak pressure to be up to an order of magnitude higher than thermal expansion [24].

The generation of pressure inside the liquid, when the beam is targeted at the stone is still not well understood but some model have been proposed in which, when beam fall on the surface of target thermoelastic expansion of the solid surface occurs, which generates mainly a shear photo acoustic pulse into solid The thermal coupling at the interface with the liquid leads to a thermal piston expansion of the liquid layer within the thermal diffusion length, but this produces weak acoustic pulse into solid owing to the weak acoustic coupling between the liquid and solid because of acoustic impedance mismatch. However, above the ablation threshold particle also come out from the sample, which scattered the acoustic wave and generates spherical wave. Due to the highly non-linear characteristic phenomenon, the exact physical mechanism is not known upto date. The theoretical description is extremely difficult due to formation of superheated liquid, thermal instability of evaporation front and development of nucleation centre. The influence of violent boiling on pressure generation has not yet to be understood.

The aim of this thesis is to use of the photo acoustic deflection (PAD) technique for the measurement of laser ablation threshold and pressure inside the liquid in presence of solid target, a gallstone and aluminum. Result of breakdown of liquid is also presented. In chapter 2 describes the experimental technique used. PAD technique and PA generation mechanism is given in chapter 3. Experimental result and discussion are given in chapter 4. In chapter 5 the summary of thesis is presented.

CHAPTER II

Experiment Techniques

The experimental arrangement for observing photo acoustic beam deflection is shown in Fig. 2.1. We have used Spectra physics (Model DCR-4G) Q-switched Nd:YAG laser and a He-Ne (Model) laser in our studies for the measurement of laser ablation threshold of Gallstone and Aluminum in liquid environment. Nd:YAG laser delivers 1 J energy in 8 nsec. (FWHM) at a fundamental with repetition rate 10 pulses/sec. The laser has a gaussian limited mode structure, the beam divergence being less than 0.5 mrad. The energy of the laser is monitored using laser power meter (Ophir Model 30A) by placing in the path of main beam. Varying the lamp energy on the laser oscillator and amplifier varies laser energy. Burn patterns taken at different energies show no significant variation in mode pattern.

The laser pulse is checked using fast photodiodes (Intel, Model AS-2, rise time < 35 Ps). The output from detector is displayed on the oscilloscope (100 MHz, TS-8123 Iwatsu) with 50 Ohms terminator and fed on to the boxcar average (SRS 250). Boxcar (SRS) is triggered externally with Q-switch synchronous pulse. The average output from the boxcar is recorded on the strip chart recorder.

The Nd:YAG laser here used is an example of four level lasers is given in fig. 2.2. In Nd:YAG laser the active medium is triply ionized neodymium (Nd^{3+}) which is optically pumped by flash lamp. The energy level diagram is given in fig. 2.3. The flash lamp is placed at one focus of an elliptical chamber for the uniform illumination of Nd:YAG rod. The main pump band for excitation of neodymium ions is in 0.81 and 0.75 μm wavelength regions. Typical neodymium ion concentrations used are of the order of $1.38\times10^{20}/\ cm^3$. The active medium is placed in a resonant cavity of two mirrors. Here a small high reflector mounted on a clear substrate lies on the optical axis of the resonator. Energy escapes the resonator by diffracting around this dot, which gives the "diffraction coupled resonator" (DCR) its name. The beam is Q-switched in order to shorten the pulse and raise its peak power. A cw He-Ne laser of power 35 mW is used as a probe beam, which passes parallel close to the target surface. As soon as pressure is generated in the liquid environment, probe beam will

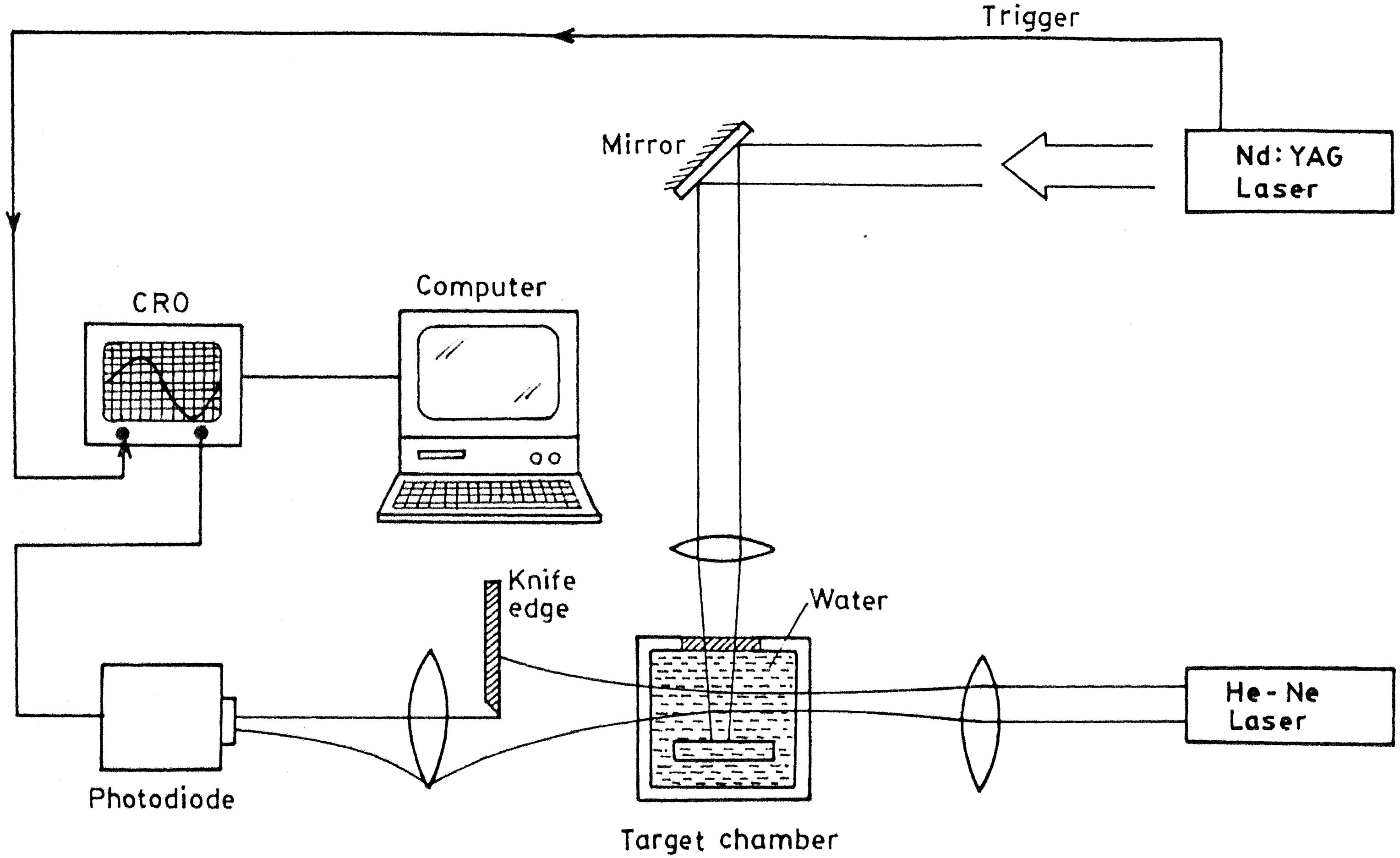

Fig. 2.1 Schematic diagram of Experimental setup for PAD.

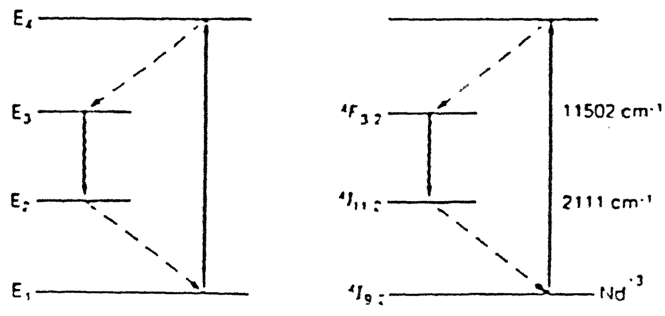

Fig. 2.2 Transition scheme of four level laser.

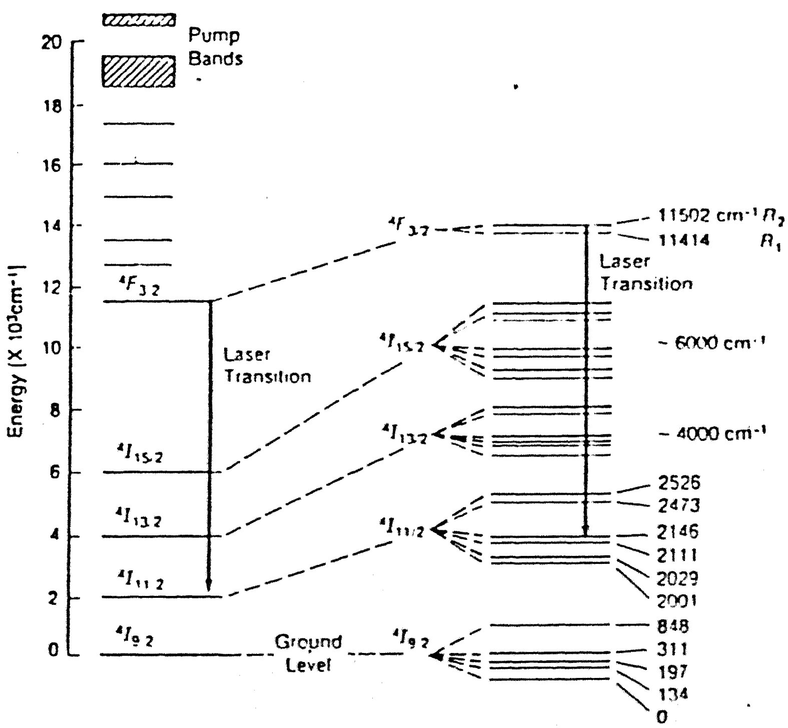

Fig. 2.3 Energy level diagram of Neodymium.

be deflected due to change in refractive index in the vicinity of the sample. Fast photodiode detector is used at a distance 2 m from the He-Ne laser to measure the angular deflection signal of the probe beam by knife-edge technique. A storage oscilloscope, which is triggered externally by Q-switch output of Nd:YAG laser is used to store photo acoustic deflection signal. The oscilloscope is interfaced with IBM PC to store all the data. The entire experiment is done in single shot mode.

The experimental set up is shown in fig. 2.1. The solid sample is placed under water, which fills a cuvette made of Kodak glass, which is transparent for infrared to UV light. The Nd:YAG laser pulse is directed on to the sample with incident angle 90°. The fast photodiode is placed normal to the laser irradiated solid surface.

CHAPTER III

Photo acoustic Detection Technique and Generation Mechanism

The photo acoustic technique is based on detecting the refractive index gradient in water induced by the change in density. The change in density can be created by temperature and pressure gradient. While crossing the probe beam, a pressure wave introduces a refractive index gradient across the probe beam waist. Therefore, the probe beam deflects towards the optically denser side, producing the so-called, mirage effect. This deflection is measured by photodetector with knife edge as shown in fig. 2.1. A He-Ne laser beam (λ = 632.8 nm) is focussed with a lens (25 cm), which passes over the Nd:YAG laser irradiated area. The focal point of this probe beam is positioned right above the centre of Nd:YAG irradiated area. The knife edge blocks, half of the probe beam at static condition, and other half is focused by lens (25 cm) onto a fast photodetector (rise time < 20 ns). The probe beam axis is one mm away from and parallel to the sample surface. Since thermal penetration depth ($\sqrt{4D\tau}$, where d is diffusion coefficient and τ is beam width) in liquid is of the order of 1 μm, the photothermal effect is negligible. Ordinary water is used as a sample liquid. The absorption coefficient of ordinary water is 0.01cm^{-1} at 1.06 μm wavelength, which is very low as compared to absorption coefficient of any metal like Al, Cr and polymer Teflon etc. Therefore one assumes that laser light is fully absorbed by the solid target (Gallstone and Al).

Photo Acoustic Generation

In principle there are five important interaction mechanisms, which can be responsible for the generation of acoustic waves: dielectric breakdown, vaporization or material ablation, thermoelastic process, electrostriction and the radiation pressure. Their contribution depends upon the parameters of the incident laser beam as well as on the optical and thermal properties of the medium.

The dielectric breakdown occurs at laser intensity above ~10^{10} W/cm^2 which can be obtained by focusing the pulsed laser of sufficient energy through the lens.

This effect has been investigated experimentally and theoretically in details for gases[25-28], liquid[26-31] and solid[25, 32]. Plasma production related to dielectric breakdown produces shock waves, which propagates initially with supersonic speed in the medium. The dielectric breakdown is the most efficient process for converting laser i.e. (optical energy) into acoustic energy. Conversion efficiency[33] can reach up to 30% in liquid. The dielectric breakdown dominates the interaction at high laser intensities, especially in transparent media where sound generation due to ordinary absorption does not occur

The second interaction, explosive vaporization in the case of liquid or material ablation in solids is responsible for the acoustic wave generation if the laser energy density within the absorbing volume of the sample exceeds a certain threshold determined by the thermal properties of the medium. The material ablation on solids is usually accompanied by plasma formation. The ejection of material from the surface involves a recoil momentum, which propagates into the bulk as an acoustic transient. For liquids the conversion efficiency can reach close to unity.[33]

For absorbing media thermoelectric process is important for the sound generation. This process is based on the transient heating of restricted volume by the absorbed laser energy. The induced temperature gradient produces a strain in the sample due to thermal expansion. This causes an acoustic wave, which propagates away from the treated zone. The thermoelastic process i.e. heating without phase change, dominates the excitation of sound in absorbing matter at laser energy below the vaporization threshold. Although conversion efficiency of n is rather low, typically $< 10^{-4}$ for liquids.[34,35] This process has found interesting, application in opto or photoacoustic spectroscopy as a sensitive method for the measurements of small absorption's in solids, liquids and gases.[36]

The electrostriction as the fourth interaction mechanism is always present due to the electric polarization of molecules in the samples, which causes them to move into or out of region of higher light intensities, depending upon positive and negative polarization. This motion produces a density gradient and consequently, a sound occurs similar to that caused by the thermoelastic processes.[37] Electrostriction, as a sound generation mechanism is only important in very weakly absorbing media, where it may limit the photoacoustic detection sensitivity. However, it has been demonstrated theoretically[38] and experimentally[39] that by using suitable time-gated

detection of the acoustic signal, strong suppression of electrostrictive component is possible. In comparison to the other sound generating mechanism the radiation pressure itself is negligible.

Three other mechanism have been omitted in this list since they play a role only under specific circumstances these are i) Photochemical effect, ii) Bubble formation and iii) Molecular dissociation.

Non-contact Optical Photo acoustic Detection

Numerous workers because of its important material testing application have studied non-contact optical probing of surface movement.[40] A general summary of non-contact ultrasonic transducers for Hutchins[41] has given nondestructive testing.

In this section we describe in some detail two general classes of techniques that have been used for non-contact optical PA detection, namely surface distortion probing and refractive index monitoring. Such non-contact techniques are useful for fast ultrasonic testing and for remote sensing of samples that are inaccessible.

A method of optical detection of photo-thermal surface distortion is developed by Amer [42] .It is based on the deflection of the probe beam reflected from the surface. PA distortion can be detected similarly. The distinction between PT distortion and PA may be described as follows: PT distortion due to thermal expansion associated with the local temperature rise follows the temperature decay via diffusion and remain close to excitation region. PA distortion on other hand propagates at a sound speed away from the excitation region. Only PA monitoring can provide sound speed and attenuation. At a distance more than several thermal diffusion lengths away from excitation region only PA distortion can be detected. Sontage and Tam[43] have extended the probe beam deflection technique of Amer, for detecting multiple reflecting PA pulse in silicon wafer excited by pulsed N_2 laser.

Another method of optical sensing of PA surface distortion is interferometry. In this case probe beam splits into two parts. One is reflected from the sample surface and another from the reference surface. The reflected beams are recombined and resultant intensity is monitored. Kino *et al*[44] have developed coherent fiber optics interferometry system for measuring acoustic waves on a polished and on rough surface. Bondarenko[45], Calder and Wilcox[46] and Hutchin and Nadu[41] have used Michelson Interferometer for detecting the PA pulse in metal plate, while Suemune *et*

al [47] have extended this work to detect photo acoustic vibration in Ga, As plate produced by focussed diode laser beam modulated at ~100Hz. Ciclo[48] has described an optical detection method of acoustic waves for characterization of sample with unpolished surfaces.

The second technique for non-contact PA monitoring relies on detecting refractive index change associated with the PA pulse. The detection of refractive variation caused by acoustic waves is not new. This method is called optical probing of acoustic refractive index gradient (OPARIG) and is applicable only for material transparent to the probe beam. Here the transient deflection of the probe beam due to traversal of the PA pulses is detected.

Quantification of the OPARIG signal S(t) have been given by Sullivan and Tam [51], using a photodiode with small active area as a fast deflection sensor (Fig.3.1). When the PA pulse produced by the excitation beam crosses the probe beam, a transient angular detection ϕ of the probe beam is produced. In order to get the relation between deflection and refractive index, we start with the fundamental definition of refractive index which is given is given by ratio of velocity of light in vacuum (c_o) to that in any medium (c),

$$n = c_o/c \tag{3.1}$$

For given substance and wavelength of light, the index of refraction is a function of density (ρ). In gases, the difference between the speed of light in vacuum and in gas is very small and directly proportional to the density of gas.

$$n = 1 + \beta \frac{\rho}{\rho_s} \tag{3.2}$$

where, ρ_s is reference density of gas at 0° C, 760 mm pressure of Hg. Equation of 3.2 may be regarded as first order approximation in a series expansion of a density of gas. The higher order term can be neglected for few dense.

Equation 3.2 shows that in an inhomogeneous, such as, flow field varying density, the index of refraction is variable. Light passing through one region of the

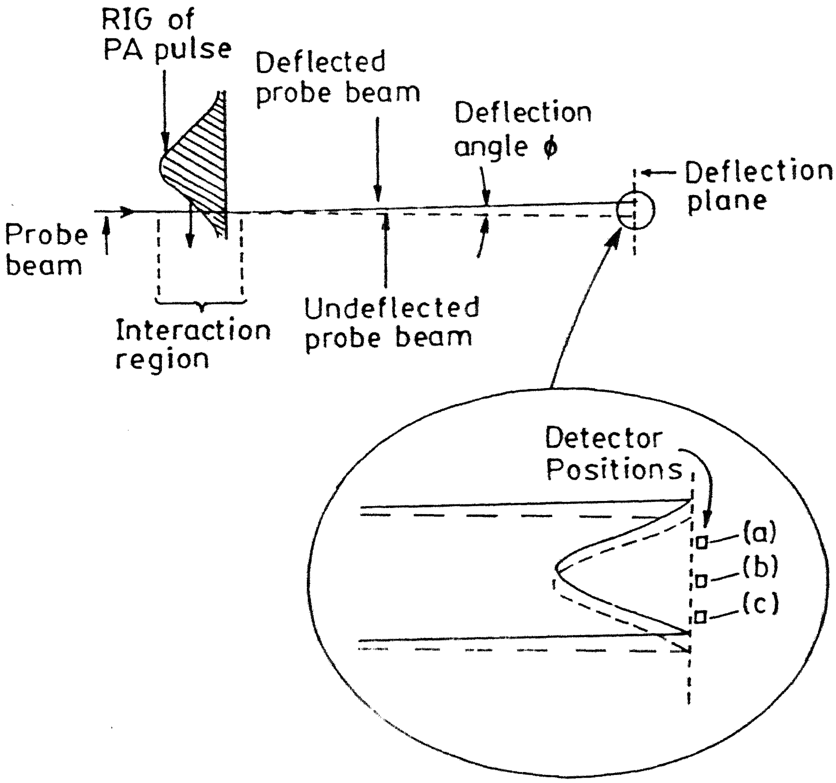

Fig. 3.1 A probe beam deflection method for non-contact transmission detection of PA pulses due to the transient deflection of narrow collimated probe beam by refractive index gradient.

field is retarded in a different way than from other region. This will make two effects on the transmitting light.

1. Turning the wavefronts, due to refractive index gradient.
2. Relative phase shift on different rays due to difference in path-length

We shall now consider the effect of refractive index that is responsible for PA beams deflection, while second effect is responsible due to interferometric process. Fig 3.2(a) shows the light traversing into field in which the density varies in the Y-direction, as indicated by the lines of constant density. The lines indicated by ω are the wavefronts and lines orthogonal to them are shown by the symbol r. For the progress of the wavefronts from the position ω_1 to ω_2,in small time interval τ, is given by

$$\tau = d\xi/c \qquad (3.3)$$

where $d\xi$, is the length traversed by light ray along the direction r_a as shown in fig 3.2(b)

If the density of the gas increases along the Y- direction r_a than that of r_b by an amount dc, this will turn the wave front of the transmitted light by an amount,

$$d\phi = \tau \frac{dc}{d\eta} \qquad (3.4)$$

The ray of light also is turned through the same angle. Then, its radius of curvature becomes,

$$\frac{1}{R} = \frac{d\phi}{d\xi} = \frac{|dc|}{c|d\eta|} = \frac{|dn|}{n|d\eta|} \qquad (3.5)$$

Now, for a varying density field as shown in figure 3.2(a) the above equation changes to,

$$\frac{1}{R} = \frac{\sin\alpha}{n}\frac{dn}{dy} \qquad (3.6)$$

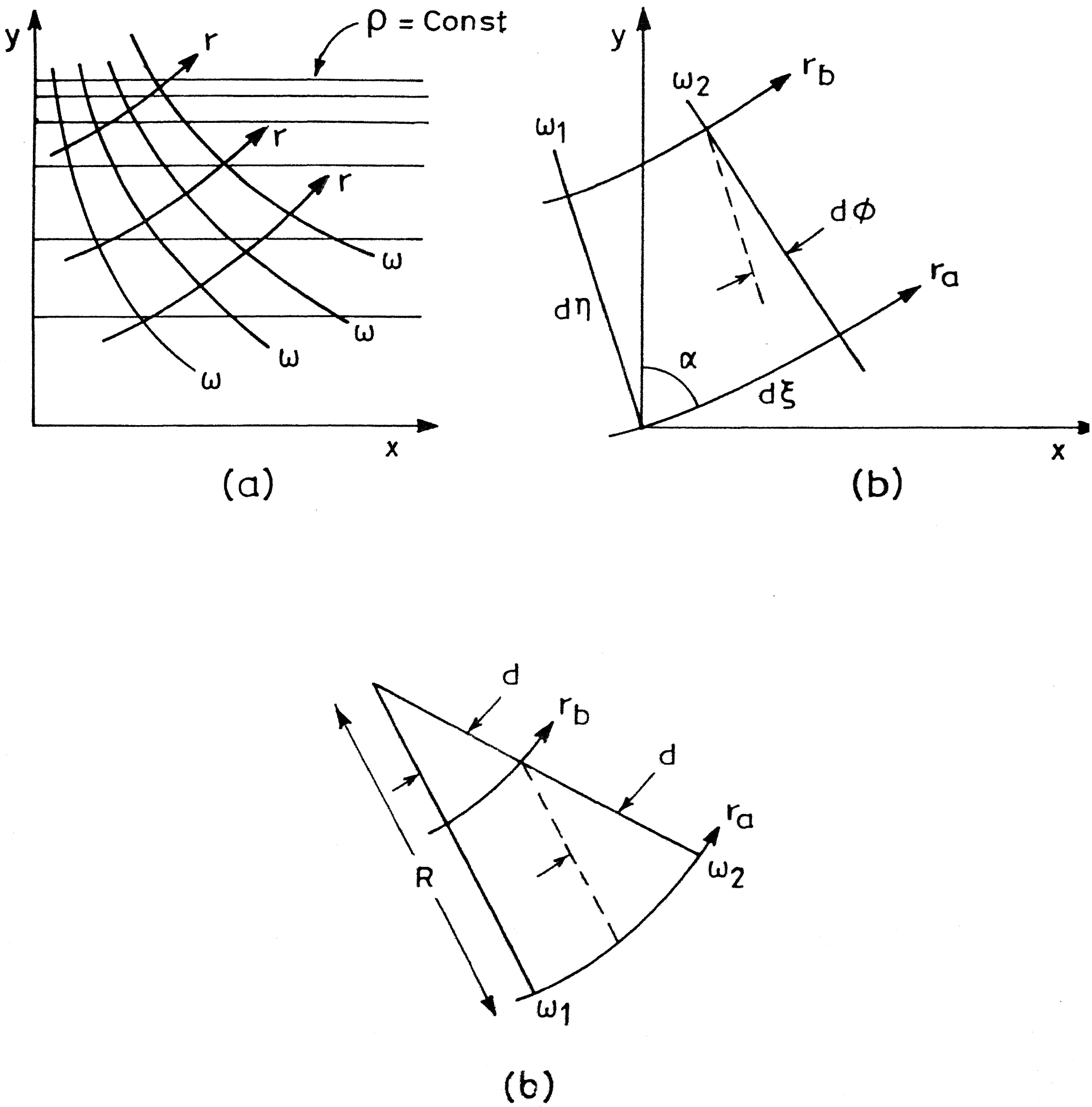

Fig. 3.2 (a) Refraction in density field. Ray (r) and wave fronts (w).

(b) Orthogonal mesh element formed by rays and wavefronts.

The total angular deflection of ray after traversing the chamber is given by

$$\phi = \int d\phi \tag{3.7}$$

The deflection of the ray is so small that the density along the curved ray is nearly the same as along the nearby path. Thus for small density gradient of the ambient gas, the expression for probe beam deflection reduces to

$$\phi = \int_o^l \frac{1}{R} dx = \int_o^l \frac{1}{n}\frac{dn}{dy} dx \tag{3.8}$$

$$\phi = \frac{l}{n_0}\frac{dn(r,t)}{dy} \tag{3.9}$$

$$\phi(r,t) = \frac{l}{n_0}\frac{\partial n}{\partial p}\frac{\partial p(r,t)}{\partial t}\frac{\partial t}{\partial y} \tag{3.10}$$

where in the above equation L is the interaction length between acoustic pulse and probe beam, n_o is the normal refractive index of the samples, $\partial n/\partial p$ is inverse of pressure gradient n(r, t) = change in the refractive index which is proportional to the PA pressure p(r,t) and l is the interaction length of the photoacoustic pulse with probe beam and $\partial y/\partial t$ is velocity of sound. Thus

$$\phi(r,t) \propto \frac{\partial p(r,t)}{\partial t} \tag{3.11}$$

The small transient probe deflection ϕ causes the probe beam to move across the detection photodiode. The observed probe beam deflection signal s(t) from the photodiode is given by

$$s(t) = GI'_p(r_d)\, L\phi \tag{3.12}$$

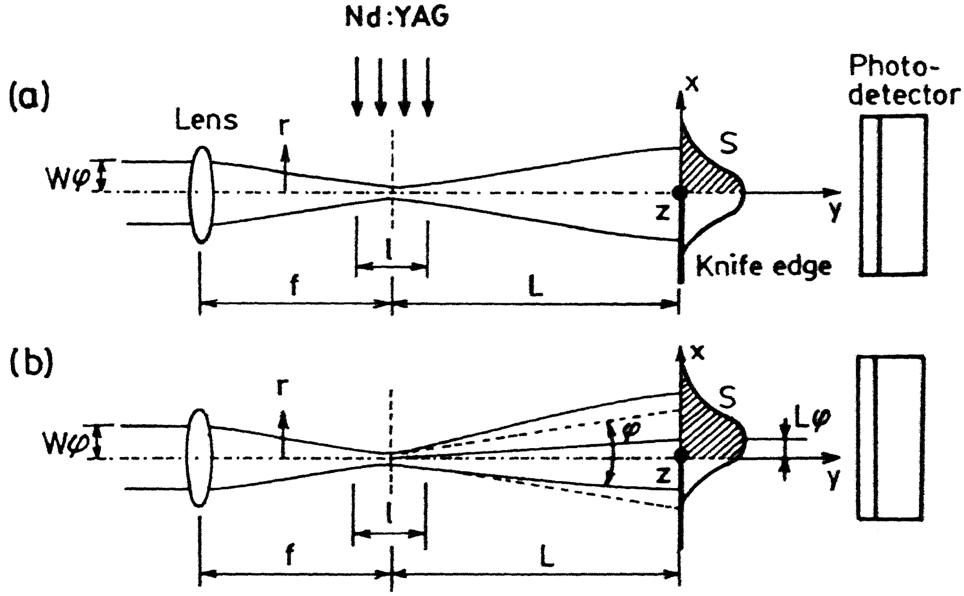

Fig. 3.3 Geometry of (a) undeflected (b) deflected probe beam with Gaussian intensity probe.

where G is constant which depends upon photo detector. sensitivity, L is distance from the interaction region in the cell to photodiode and $I_p(r_d)$ is the lateral spatial derivatives of the probe beam intensity distribution at the photodiode position r_d.
Equation (3.12) implies:

$$s(t) \propto \phi \tag{3.13}$$

therefore from equation (3.11),

$$s(t) \propto \frac{\partial p(r,t)}{\partial t} \tag{3.14}$$

Thus, the experimental probe-beam deflection signal is a measure of time derivative of the PA pulses of the probe beam position. Sullivan and Tam [51] have used OPARIG for reliable determination of PA pulse profiles generated by laser beam duration in the μs or ns. Thus, optical method of PA profile monitoring should open up new non-contact ultrasonic velocity, relaxation, and dispersion measurements. For example chemical reaction, nucleation, precipitation, and some other changes in a system frequently result in change in ultrasonic absorption or dispersion spectra detectable by monitoring the profile of the probe beam-deflection signal at a several propagation distances.

Other PA detection techniques are also possible, which make the use of detectors such as Electromagnetic Acoustic Transducer, Laser Doppler Vibrometer, Ultrasonic Doppler Vibrometer, Bragg's Scattering and etc.. Indeed almost all-acoustic sensors can be adopted for PA detection, with proper care taken for the sensitivity and detection bandwidth. For example Wilkin[52] have used Electromagnetic Acoustic Transducer to detect PA polarized shear waves, produced by laser line source. William[53] have used Bragg's scattering of a probe that is collimated with a modulated pump beam for high-frequency PA detection.

The present work aims to measure the pressure and ablation threshold of Al and gallstone in liquid environment using knife- edge experiment and the breakdown threshold of water. In detection scheme, knife edge blocks the lower half of the probe

beam (Fig.3.3). The signal received by a photodetector, S using eqn. (3.1), is written as

$$S= K[1 + \mathrm{erf}\,(\sqrt{2}\,\pi\phi/\lambda\,)] \qquad (3.15)$$

where K is gain constant and can be determined by initial signal when the deflection is zero, $S_0 = K$, therefore the deflection angle is

$$\phi = (\lambda/\sqrt{2}\,\pi\omega)*(\mathrm{erfinv}\,(1- S/S_o)) \qquad (3.16)$$

Beam waist

$$W = 2\lambda f / \pi 3\omega_e \qquad (3.17)$$

where f is the focal length of the lens and ω_e is beam radius of the lens. The beam radius is defined as the point at which the electric field amplitude has fallen to 1/e of axial value. The theoretical beam waist in air is calculated at λ = 632.8 nm and ω_l = 1340 μm, to be 7.5 μm. While experimental measurement is around 11.2 μm. This discrepancy may be due to the spherical aberration of the lens, and optical misalignment. The beam waist is expected to be different in liquid from that of air.

The depth of the focus is calculated to be 0.24 mm with w = 11.2 μm. Consequently spot of the Nd:YAG laser is confined only within the depth of the focus ± 0.24 mm, in order for the probe beam to be capable of detecting plane wave propagation without temporal distortion or spreading.

Fig 3.4 and 3.5 depicts the procedure for deriving the pressure from the deflection. Fig 3.4(a) and 3.5(b) show the deflection signal detected by photodetector for a Nd:YAG laser fluence, F = 25 J/cm^2 and 56 J/cm^2 for Al and Gallstone respectively. The trace shown in Fig 3.4(b) and 3.5(b) are the deflection angle ϕ computed using the eqn. 3.16. The deflection angle ϕ is easily converted to dP/dt by using eqn. 3.1. The dn/dp value is 0.00015 Mpa^{-1} for water at λ = 632.8 nm, and the speed of sound 1481 m/s. Finally pressure p(t) can be obtained by integrating with respect to time fig. (3.4(c)and 3.5(c))

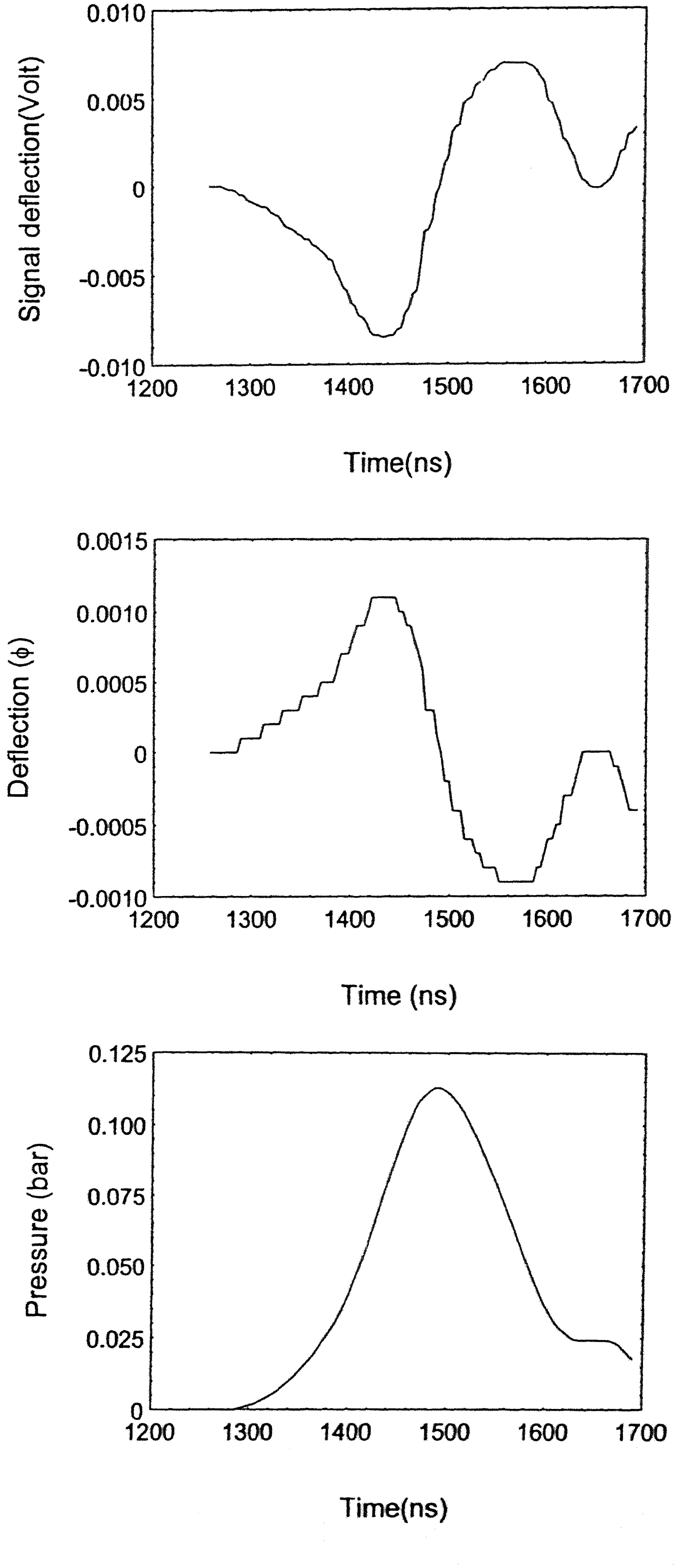

Fig. 3.4 The deflection signal received by the photo detector (a)for aluminum in water with the Nd:YAG laser fluence 25 J/cm^2. Also shown are (b)

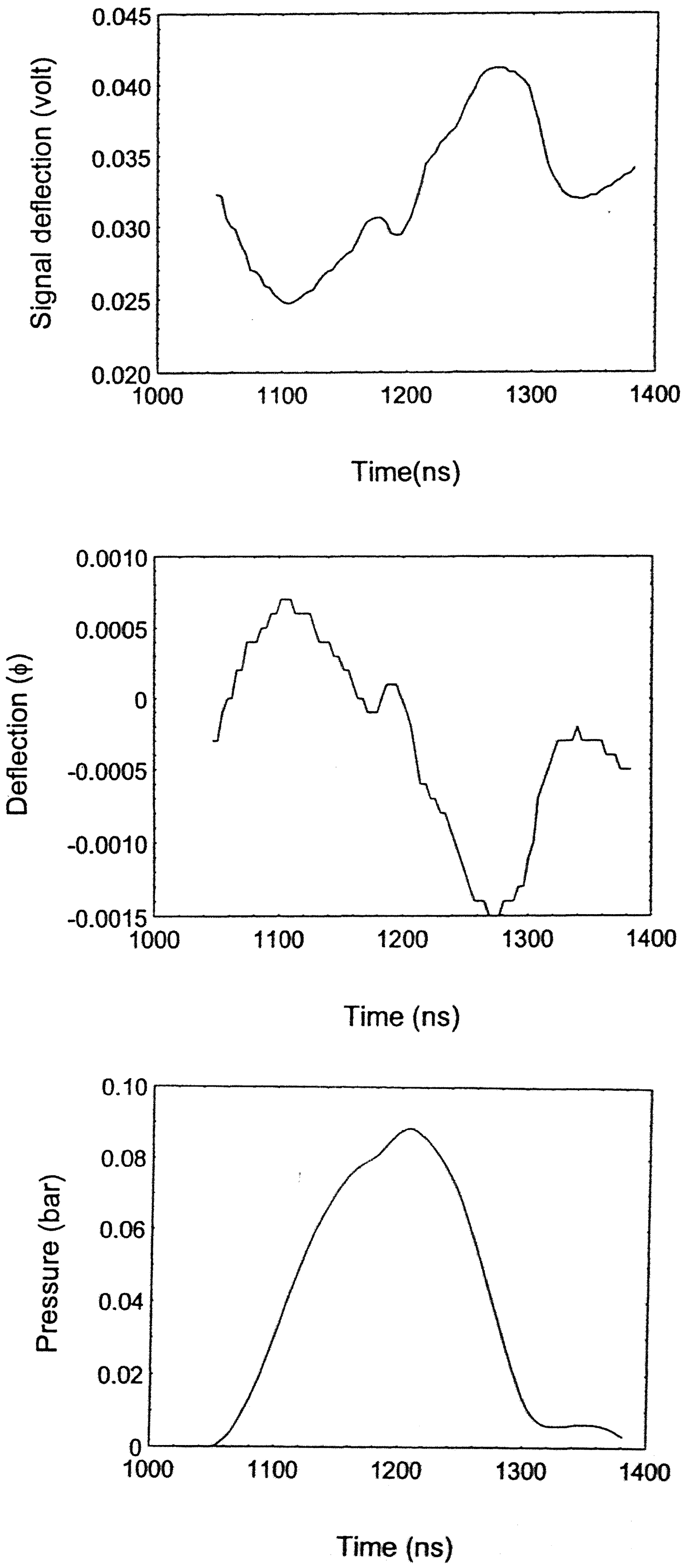

Fig. 3.5 The deflection signal received by the photo detector (a) for Gallstone in water with the Nd:YAG laser fluence 56 J/cm^2. Also shown are (b)

Other acoustic detection techniques are: (a) Microphone (b) piezoelectric transducer (c) fiber optics sensor etc.. Non-contact detection technique is better than above mentioned technique because these are limited to far distance (>1cm) from the irradiated source owing to relatively large size; also, the accurate detection of the transient photoacoustic pulse shape is difficult because of transducer ringing and the lack of bandwidth. In addition they are applicable only to certain thin sample. However, non-contact PA technique is applicable to any opaque solid of any width. Also, the probe beam can set for small distance (<1 mm) from the photo acoustic source so that excessive damping of the high signal can be avoided.

CHAPTER IV

Result and discussion

Measurement of laser ablation threshold

The PAD technique to measure laser ablation threshold has been discussed in chapter 3. Experimental setup is given in fig 2.1. Here the results obtained about the laser ablation thresholds for various targets in ordinary water are presented. The technique essentially consist of measuring the deflection of optical probe beam, a low power He-Ne laser in present work, due to the refractive index gradient in the vicinity of the sample surface irradiated by a pulsed Nd:YAG laser. Targets used in the present work are

1. Aluminum
2. Gallstone

Determination of Ablation Threshold using 1.06 μm Irradiation

To measure the ablation threshold of material the following experiment was performed. The photo acoustic probe beam axis is moved away from the sample (X-direction) and parallel to the surface (Z-direction) as shown in fig. (4.1). In original configuration, fig. (4.1a), probe beam passes over the center of Nd:YAG laser spot, and the focal point of the probe beam is focussed outside the Nd:YAG laser focus spot. In fig. (4.1b) where the probe beam passes over the edge of the sample, without any diffraction effect, the pressure wave propagates only in the direction normal to the surface. In this condition the probe beam will not be deflected. Signal detected above and below threshold fluence is shown in fig.4.2. When the Laser fluence was less than the threshold, no pressure is detected by off centered probe beam as shown in fig 4.2 (b) but at the same fluence we observed the deflection at center spot according to fig 4.2 (a). This supports the one dimensional thermoelastic pressure generation. However, if the laser fluence is greater than the threshold, then a pulse is detected for off axis position as shown in fig 4.2 (c). Fluence at which we get the deflection is the ablation threshold of the material. For aluminum the ablation threshold (Fig 4.3) measured by this method in water is 22.2 J/cm^2 and for gallstone, it is 20 J/cm^2.

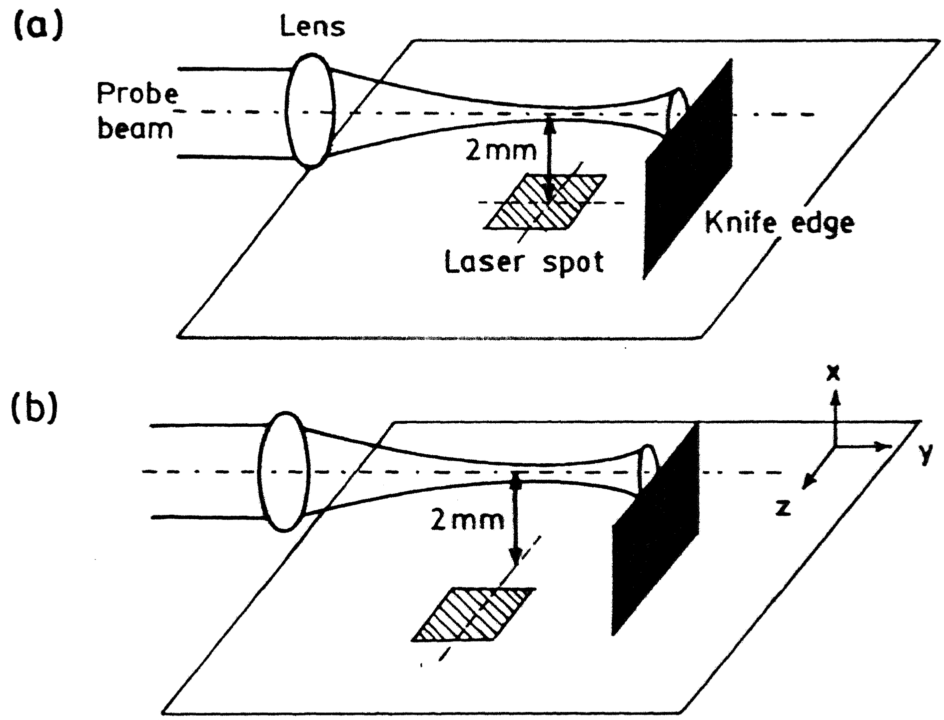

Fig. 4.1 The experimental setup for PA probe beam deflection technique with (a) original probe beam configuration and (b) the probe beam at the off the axis

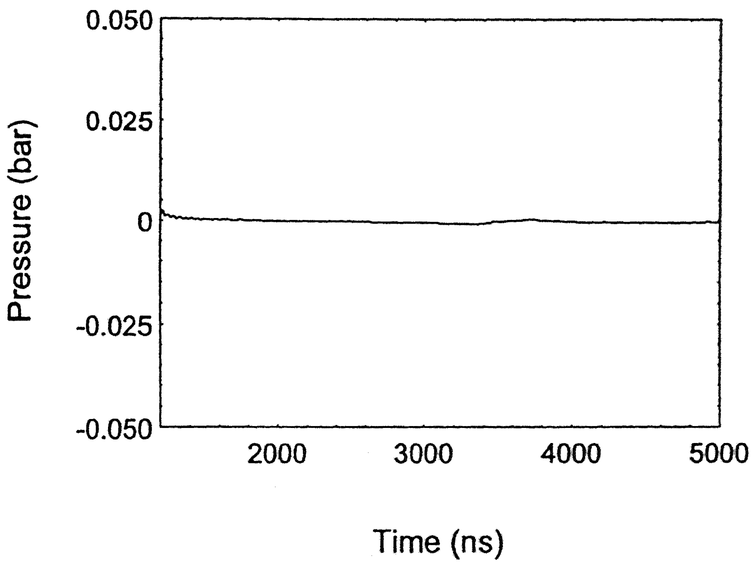

Fig. 4.2 (a) Variation of off axis Photo Acoustic Deflection Signal with time for Gallstone in water at 18.1 J/cm^2 laser fluence.

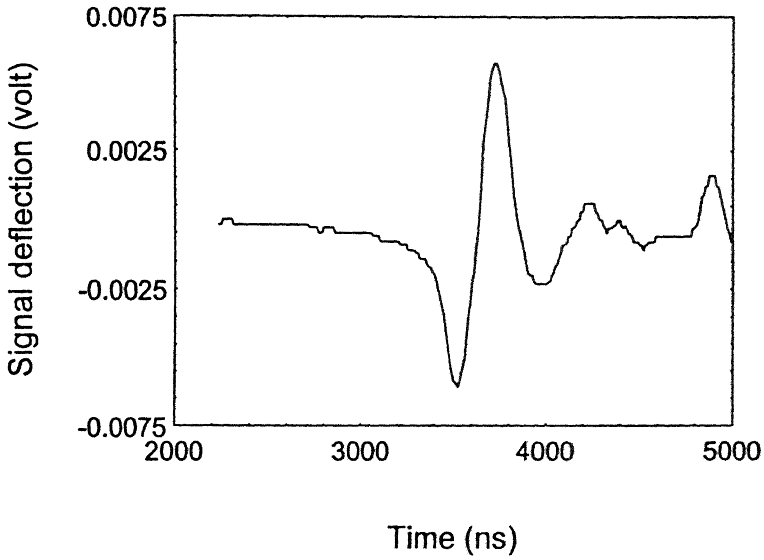

Fig. 4.2 (b) Variation of on axis Photo Acoustic Deflection Signal with time for Gallstone in water at 18.1 J/cm^2 laser fluence.

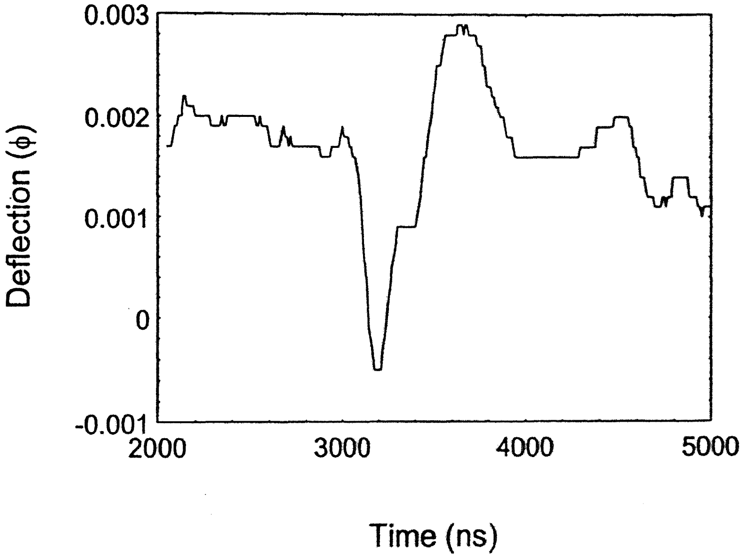

Fig. 4.2 (c) Variation of off axis Photo Acoustic Deflection Signal with time for Gallstone in water at 22 J/cm^2 laser fluence.

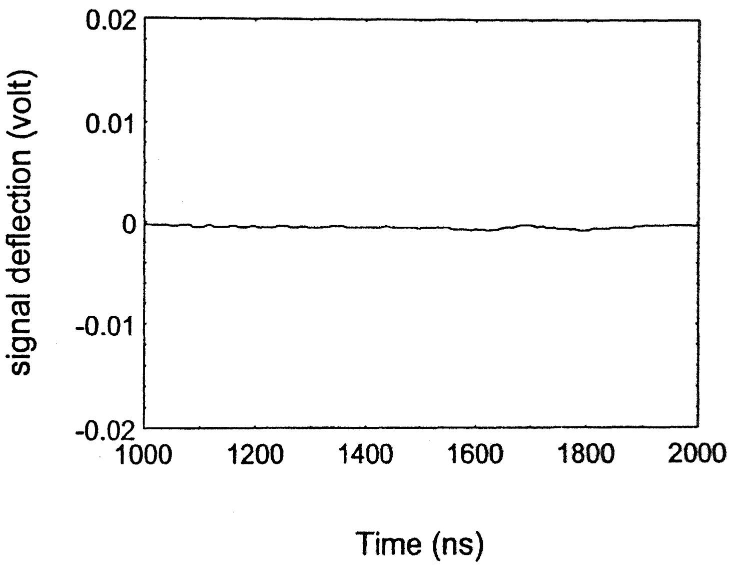

Fig. 4.3 (a) Variation of off axis Photo Acoustic Deflection Signal with time for aluminum in water at 18.1 J/cm^2 laser fluence.

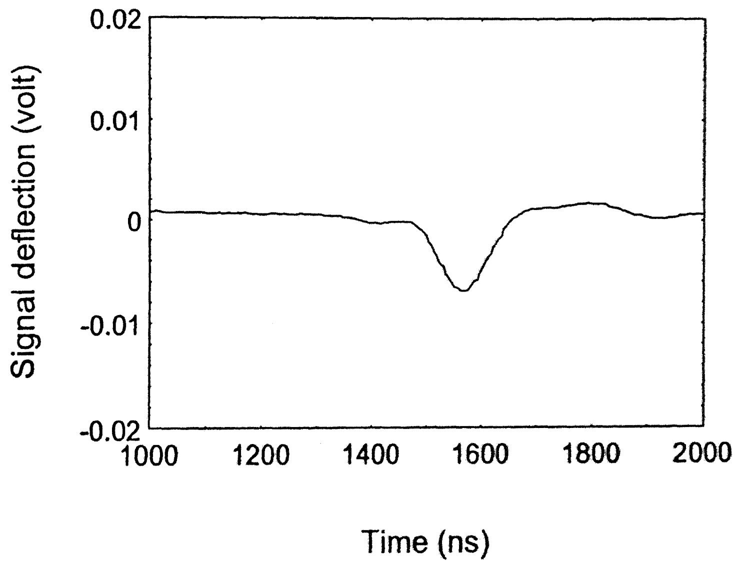

Fig. 4.3 (b) Variation of on axis Photo Acoustic Deflection Signal with time for aluminum in water at 18.1 J/cm^2 laser fluence.

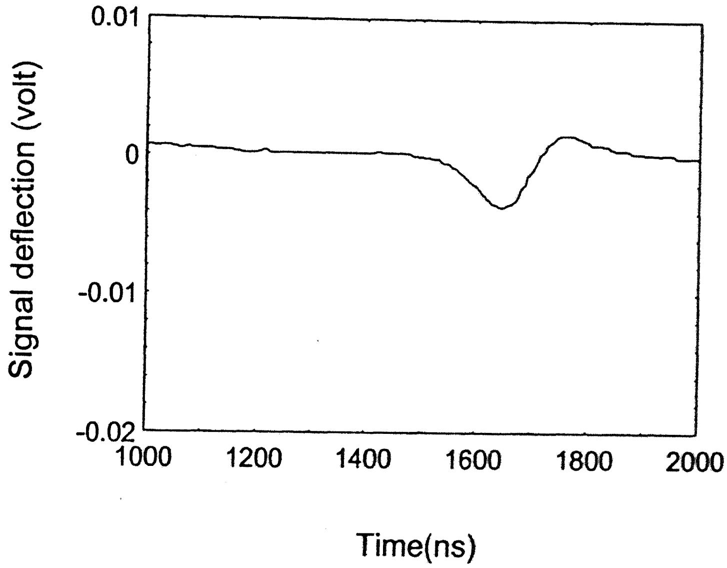

Fig. 4.3 (c) Variation of off axis Photo Acoustic Deflection Signal with time for aluminum in water at 22.2 J/cm^2 laser fluence.

Transient pressure (temporal variation of pressure pulse) detected by PA deflection method is shown in fig. 4.4. It is observed that a pressure pulse of width ranging from 100 to 200 ns is generated by laser irradiation. It is however noted that tighter focusing of the probe beam and reduction of interaction length will improve the temporal resolution of the technique. The comparison of the measured pressure amplitudes did not show a strong dependence on probe beam radius. This can be explained by the fact that tighter focusing of a probe beam i.e., smaller f-number also decreases the depth of focus of probe beam. The two competing effect, i.e., tighter focus versus decrease depth of focus, tend to cancel each other. It is however observed that the decrease of laser irradiated area, i.e., the decrease of interaction length, improve the deflection signal. This is an experimental requirement that the Nd:YAG laser beam width should be smaller than that of the depth of focus of probe beam.

The signature of the pressure pulse is investigated at various fluences. When laser fluence is low i.e., below the ablation threshold, the pressure is generated thermoelastically. When the laser fluence exceed the ablation threshold, there exist another contribution to the pressure due to the stemming of material and the bubble growth in liquid due to the breakdown of water. The observed signal is superposition of thermal expansion induced pressure, shock wave pressure and bubble-induced pressure. Thermoelastic pressure is generated by the rise in temperature. The generated pressure is of narrow temporal width, since it depends upon laser pulse width. On the other hand, pressure generated above the threshold has longer temporal duration, scaling with the bubble growth and shock wave time. Therefore, it is expected that contribution from bubble growth and ablation of material would prolong the pressure pulse at higher fluence. Indeed the widening of the pressure is observed experimentally in fig.4.4 as laser fluence increases. Figure 4.4 and 4.5 show the variation of pressure pulse width (FWHM) 163, 172 and 191 ns with laser fluences 25, 60 and 105 J/cm^2 respectively for gallstone and those for Al are 110, 121 and 153 ns respectively for the same laser fluences.

Fig 4.6 shows the variation of maximum pressure with fluence. It is observed that at initial (low) fluence there is no deflection, i.e., maximum pressure is zero, because all the energy is absorbed by the material itself. As the fluence increases deflection of signal increases because of the generation of shock waves and also due

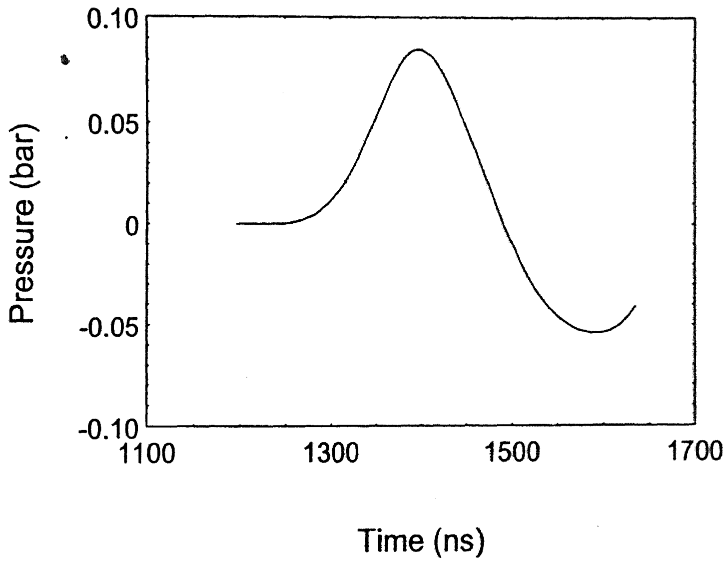

Fig. 4.4 (a) Variation of pressure generation for Gallstone in water at 25 J/cm^2 laser fluence.

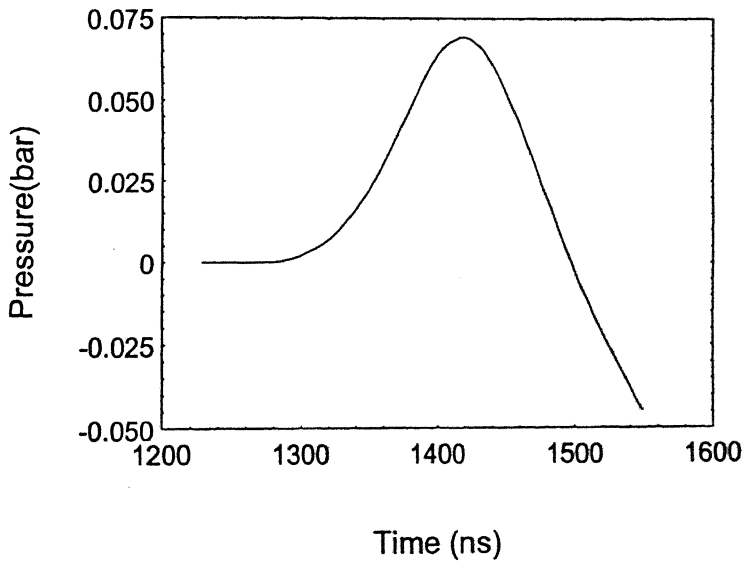

Fig. 4.4 (b) Variation of Pressure generation for Gallstone in water at 60 J/cm^2 laser fluence.

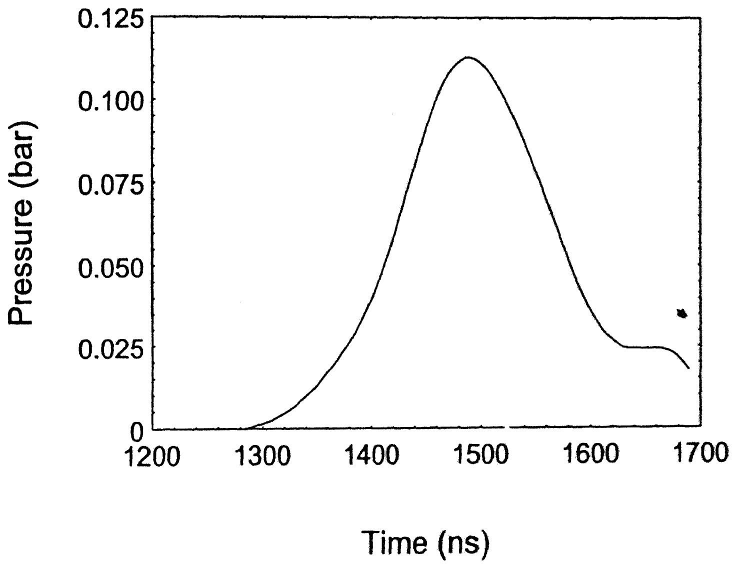

Fig. 4.4 (c) Variation of Pressure generation for Gallstone in water at 105 J/cm^2 laser fluence.

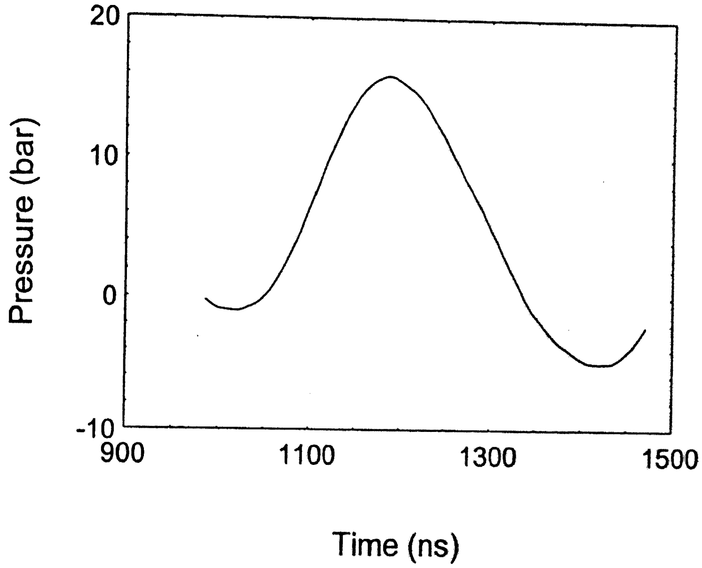

Fig. 4.5 (a) Variation of Pressure generation for aluminum in water at 25 J/cm^2 laser fluence.

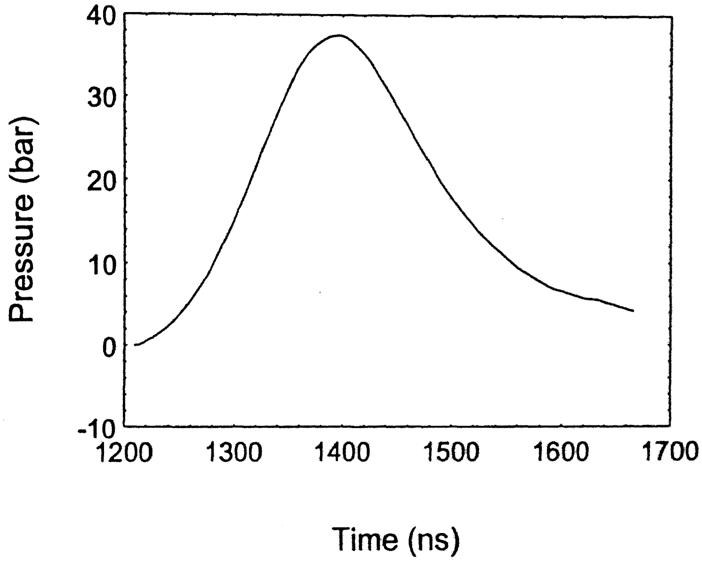

Fig. 4.5 (b) Variation of Pressure generation for aluminum in water at 60 J/cm^2 laser fluence.

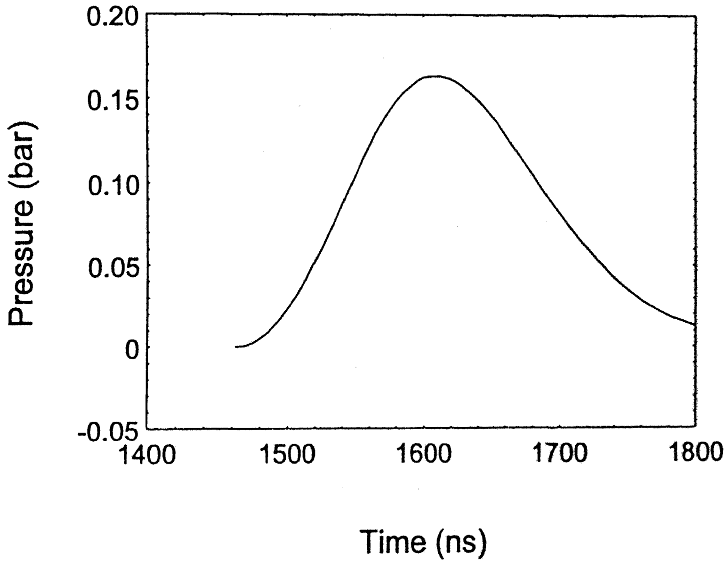

Fig. 4.5 (c) Variation of Pressure generation for aluminum in water at 105 J/cm^2 laser fluence.

to the breakdown of water. The cumulative effect of these two, show sudden increase in the pressure. As we increase laser fluence, curve become saturated i.e., pressure remains constant because of saturation in the number of bubbles on the surface and by the poor transmission of thermoelastic pressure into water. At this laser fluence, it is expected that bubble can grow large enough to agglomerate and build a continuous vapor layer on the solid surface. Consequently, the peak amplitude of pressure generated by bubbles stop growing. As the fluence increases, particles coming out also increases and hence pressure should increase but due to the scattering and diffraction net effect does not change i.e., pressure remains constant. However, as soon as fluence starts increasing, the scattering effect dominates over other things so pressure decreases with increasing fluence. This effect is shown in fig. 4.6 and fig. 4.7 for both gallstone and aluminum. For gallstone (fig. 4.6) we observed only initial zero pressure, then sudden increase in pressure and then after plateau region. We could not see the lowering of signal/pressure due to the experimental constraints (i.e. at very high fluence gallstone break.). However, for Al (fig. 4.7), we could not see the plateau region because of inner property of metal. This may be due to the fact that metal contains generally only one type of bonding. The plateau region may be very small in Al which can be measured by changing fluence in very small steps which is not feasible in the present setup. Once the material starts coming out from the surface of the metal, it will scatter as well as absorb the probe beam. Hence signal becomes weak with the increasing fluence. We can determine the ablation threshold from the points of sudden increase of pressure in fig. 4.6 and fig. 4.7. The ablation thresholds obtained for gallstone and aluminum are 25 J/cm^2 and 24 J/cm^2 respectively. Variation of deflection signal is also investigated at various laser fluences. We obtained the same results for aluminum and gallstone as shown in fig. 4.8 and fig. 4.9.

Variation of Pressure with Distance at Constant Fluence

In this experiment we focused the incident laser beam at the target and then varied focusing distance from the target, keeping probe beam at a fixed distance from the target. Observed variation of pressure with distance is given in fig. 4.10, 4.11, 4.12 and 4.13 for Al and Gallstone with fluences 60, 105 and 150 J/cm^2. The general trend may be explained as follows: when the laser is focused at the target, material is

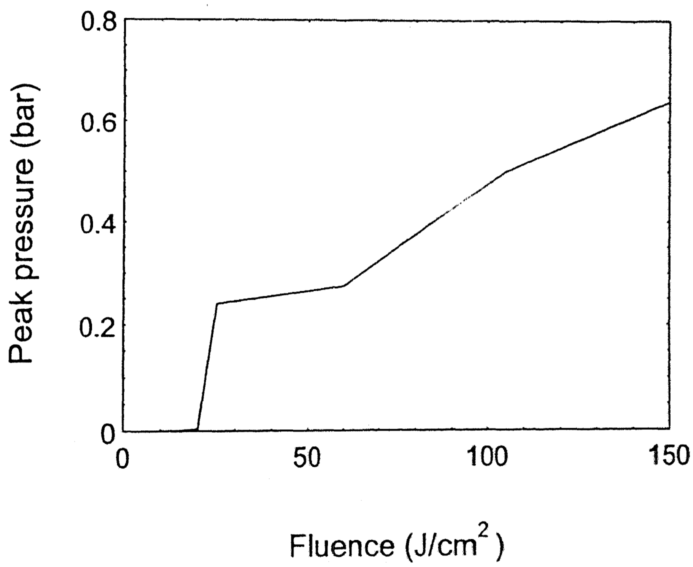

Fig. 4.6 Variation of Peak Pressure generation for Gallstone in water at different laser fluence.

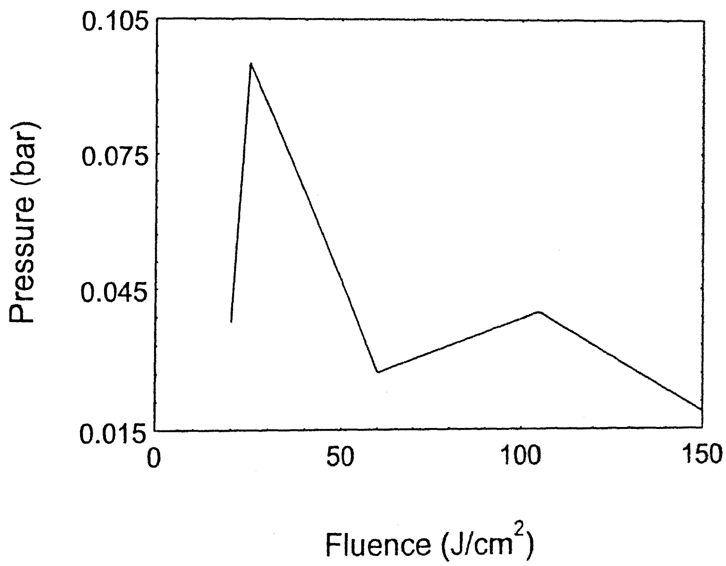

Fig. 4.7 Variation of Peak Pressure generation for aluminum in water at different laser fluence.

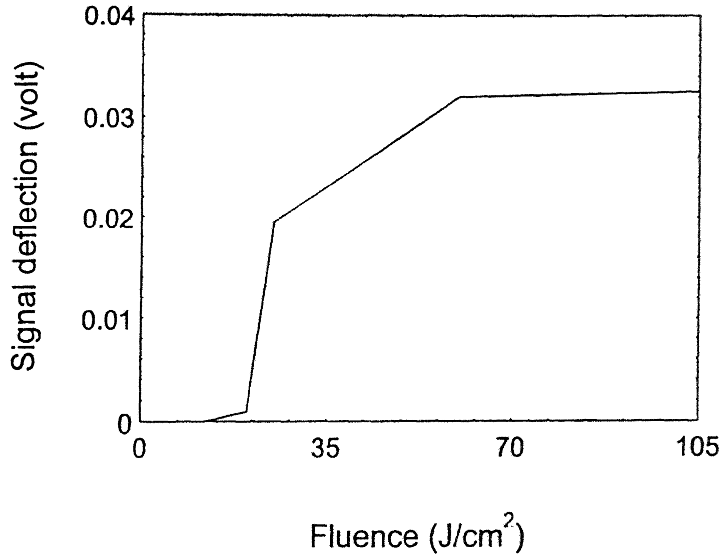

Fig. 4.8 Variation of Signal deflection aluminum in water at different laser fluence.

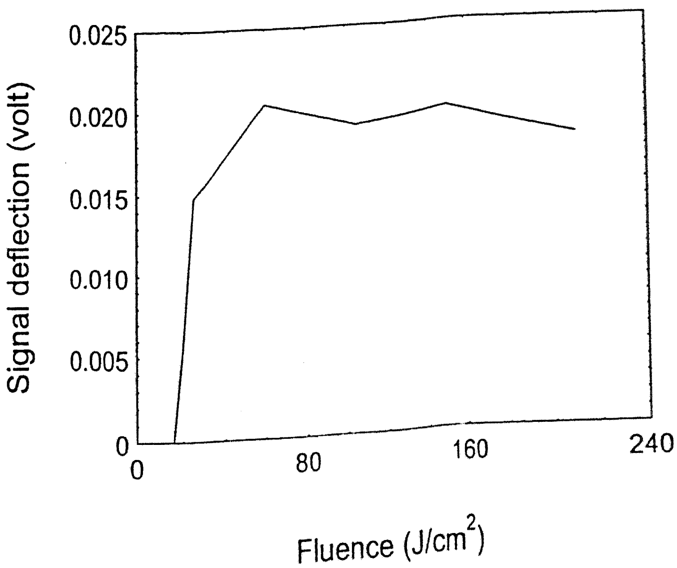

Fig. 4.9 Variation of Signal deflection Gallstone in water at different laser fluence.

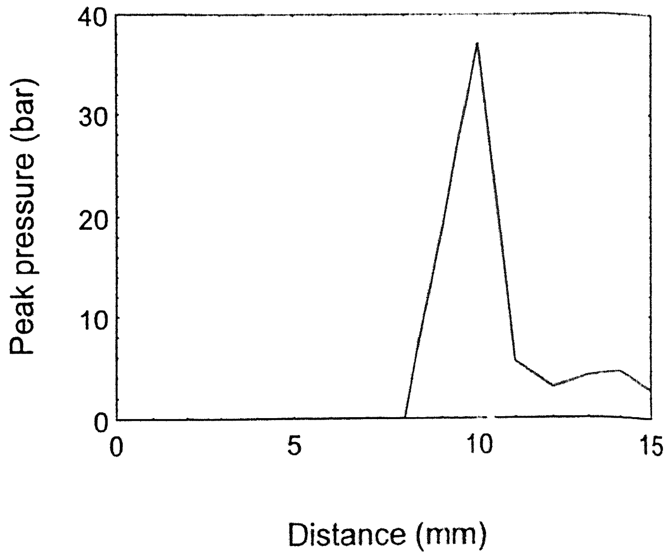

Fig. 4.10 Variation of Peak Pressure at the different focal points of the pump beam from the target surface of Al at 25 J/cm^2 laser fluence.

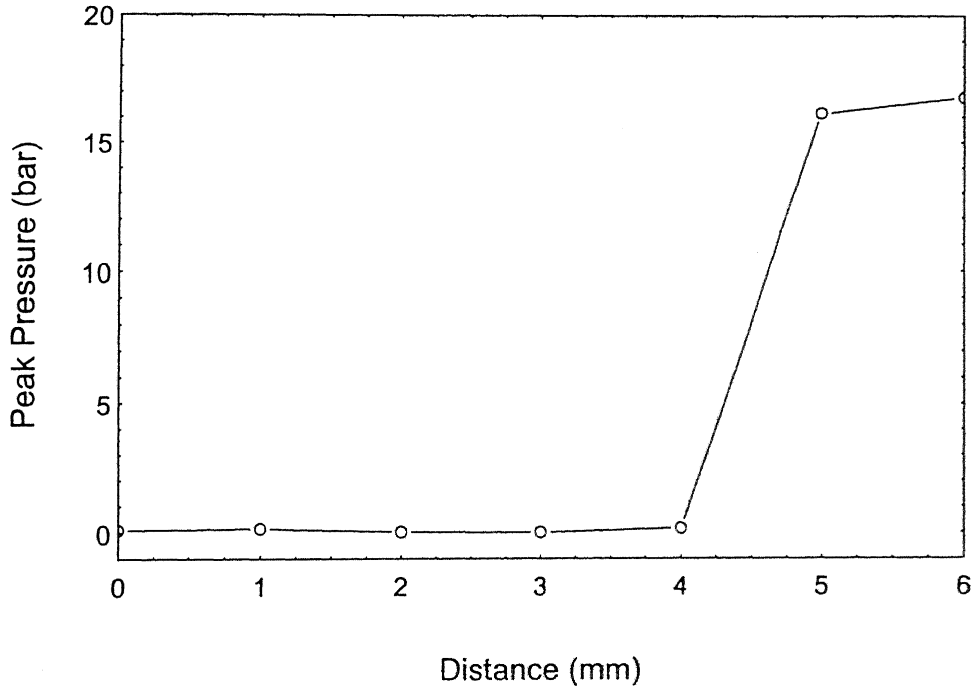

Fig. 4.11 Variation of Peak Pressure at the different focal points of the pump beam from the target surface of Gallstone at 60 J/cm^2 laser fluence.

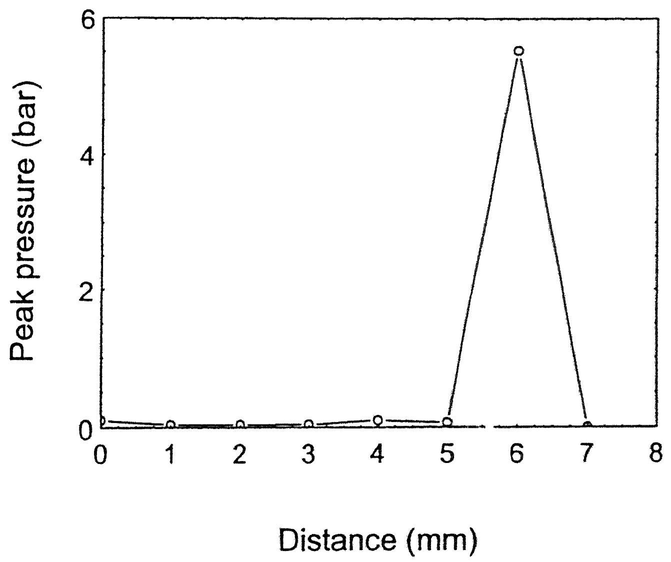

Fig. 4.12 Variation of Peak Pressure at the different focal points of the pump beam from the target surface of Gallstone at 105 J/cm^2 laser fluence.

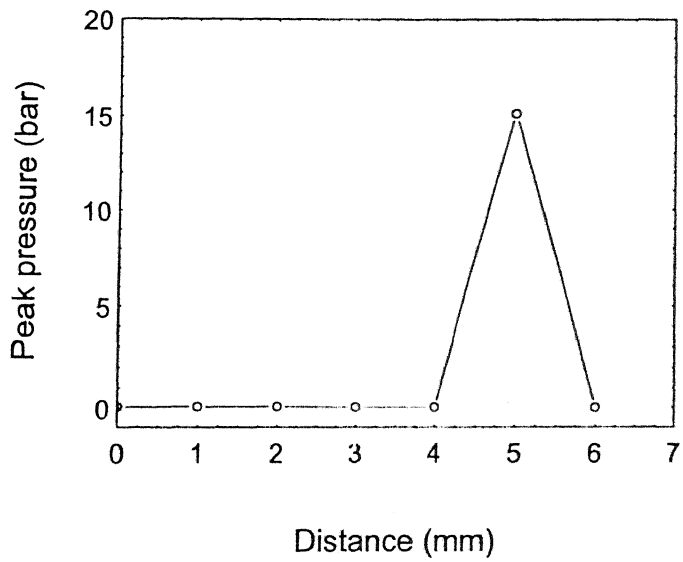

Fig. 4.13 Variation of Peak Pressure at the different focal points of the pump beam from the target surface of Gallstone at 150 J/cm^2 laser fluence.

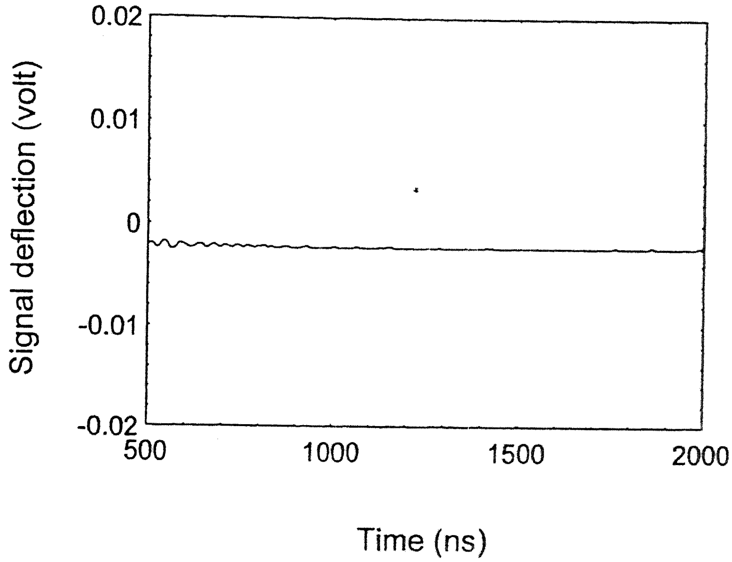

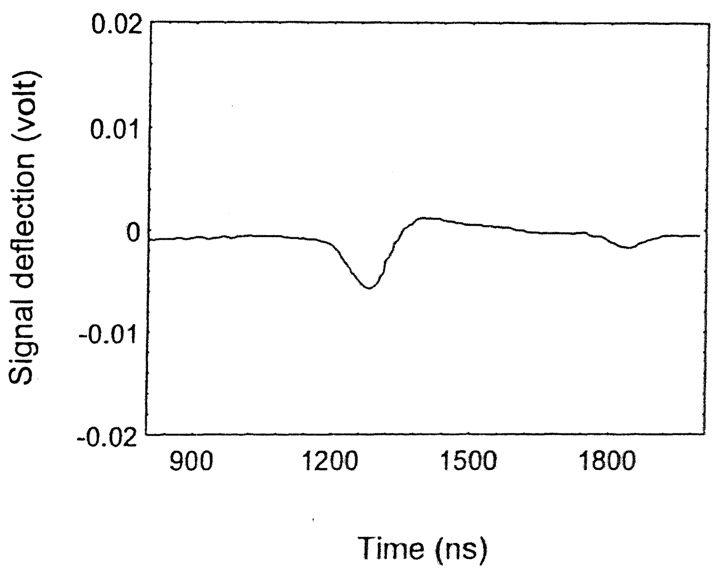

Fig. 4.14 (a) Variation of Photo Acoustic Deflection Signal with time in water at 40 J/cm^2 laser fluence (b) Variation of axis Photo acoustic Deflection Signal with time 56 J/cm^2 laser fluence.

ejected out and because of scattering of the probe beam, its signal becomes low. But as the laser is focused away from the target surface, no ablation of the material will take place, but since the laser is focused in water there will be bubble formation. When these bubbles break they give rise to pressure wave which results in large deflection in probe beam. However, if the focused laser beam is very far from the target surface these pressure wave die out or becomes very weak (before reaching the probe beam) hence the deflection observed will be very low

Determination of Threshold Breakdown of Water

For the determination of breakdown of water we performed an experiment in which incident laser light is focused in water and probe beam passes 2 mm away from the focused point. At low fluence we observed no deflection in probe beam as shown in fig 4.14(a), but as we increased the fluence above 56 J/cm^2 we observed the deflection (fig. 4.14(b)) which correspond to the threshold breakdown of water. This assumption is because of the fact that the spherical waves cannot be generated without the breakdown of water. Laser induced breakdown in liquid is mainly of interest in the medical laser application, such as intraocular photodisruption, where it is used for the evaporation of transparent tissues.

We performed the experiment using defocused laser beam but we were unable to get any deflection at the available energy. If we can break the gallstone without the help of the focused beam then we can correlate the laser-induced fragmentation with conventional fragmentation of gallstone.

CHAPTER V

Conclusions

We measure the ablation threshold for Gallstone and aluminum in water by using Photoacoustic Deflection Technique. The ablation threshold of gallstone is 20 J/cm^2 and for Al is 22.2 J/cm^2. We report the detection of the acoustic pulse generated in water, during the interaction of laser with aluminum and Gallstone. This technique is also used to carry out the calculation of the absolute pressure generated in water. It is observed that the pulse width of the pressure wave increases with the increasing laser fluences. Observed FWHM is ranging from 100 to 200 ns. FWHM of Gallstone is higher than the Al. The Results of the variation of pump beam's focal spot from the target surface shows first the increment and then the decrement in peak pressure pulse. Diffraction effects in water also influence the probe beam deflection signal. It is observed that above the ablation threshold photoacoustic deflection signal starts decreasing because of the scattering effect of the probe beam by the ablation particles in water. Threshold breakdown of water is also calculated. The observed value is 56 J/cm^2. No result has been observed with the defocused laser beam because of the low laser fluence.

Future Scope of Work

The work finds its importance in the field of medical application of lasers for e.g. laser lithotrispy, corneal surgery, angioplasty. The acoustic pressure can be calculated and be optimized to define the damage threshold for the gallstone. One can extend the above work for other practical as well as theoretical understanding.

References:

1. A. Oravsky, R. I. Esenaliev, and V. S. Letokhov, (Ed.) J. C. Miller and Haglund Jr., *Laser Ablation Mechanism and Application*, Springer-Verlag, **389**, 112 (1991).
2. D. Albagli, L. T. Perlman, G. S. Janes, C. von Rosenberg, I. Itzkan, and M S. Feld, Laser in Life Science, **6** (**1**), 55 (1994).
3. I. Itzakan, D. Albagli, B. J. Banish, M. Dark, C. Von Rosenberg, G. S. Janes and M. S. Feld, AIP conf. Proceed. **288**, 491 (1994).
4. R. S. Dirges, R. J. Scallion, (Ed.) J.C. Miller and R. V. Haglund Jr., *Laser Ablation Mechanism and Application*, Spring Verlag **389**, 180 (1991).
5. R. S. Dirgus, and R. J. Scammon, *Laser Tissue Interaction II,* SPIE **1427**, 54 (1991).
6. E. Brain, C. C. Thomas, *The prepration of Decalcified sections,* Springfield. III (1966).
7. M. Borysenko, J. Borysenko, T. Beringer, T. A. Gustafson, *Functional Histology*, Little, Brown and Company, Boston (1979).

8. M. Sigrist and F. K. Kenubuhl. App. Phy. **2**, 43 (1973).
9. H. K. Park, C. P. Grigoropoulous, W. P. Leung, and A. C. Tam, IEEE Trans. Comp. Package manufac. Technol. **17A**, 631 (1994).
10. A. Vogel, P. Schweigen, A. Priece, M. N. Asioy and R. Birngurber, IEEE J. Q electron. **26**, 2240 (1990).
11. P. Teng, N. S. Nishioka, R. R. Anderson and T. F. Deustsh, App. Phy., **B42**, 73 (1987).
12. C. B. Scruby and L. E. Drain, *Laser Ultrasonic*, (Adam British 1990) ch 5.
13. A. C. Tam, Nhan Do, L. Kless, P. T. Leung and W. P. Leung, Optics letter **24**, 1809 (1992).
14. D. L. Singleton, G. Pareshkevopous, Taylor and R. S. Higginson, IEEE J. Q electron.1772 (1987).
15. Y. Tomita and A. Shima, J. fluid Mech. **169**, 535 (1986).
16. Ell Ch., F. Wondrazek, F. Frank *et al. Endoscopy* **18**, 95 (1986).

17. Ell Ch., Hockbergets J. Muller *et al. Endoscopy* **18**, 92 (1986).

18. N. S. Nshioka, and R. R Anderson, *Endoscopy* **32**, 157 (1986).

19. P. Teng, N. S. Nshioka, R. R. Anderson, and T. F. Deutsch, App. Phy. B **42**, 73 (1987).

20. P. Teng, N. S. Nshioka, R. R. Anderson, and T. F. Deutsch, Laser Life Science, **1**, 231 (1987).

21. P. Teng, N. S. Nshioka, R. R. Anderson, and T. F. Deutsch,.IEEE J.Quantuam electron. QE-**23**, 1845 (1987).

22. S. Thomas, J. Barreton, and P. Oheart, *International Conference on Photo-dynamic Therapy and Medical Laser Application* (1988).

23. L. M. Lyanshv and K. A. Mangolnykh, Sov. Phy. Acoustic **27**, 357(1982).

24. V. S. Teslenko, Sov. J. quantum electron. **7**, 981 (1977).

25. J. A. Sigrist, Phy. **60**, R83 (1986).

26. M. Sigrist and F. K. Kenubuhl, J Acoustic. Soc. America **64**,1652, (1986).

27. J. F. Ready, *Effect of high power laser radiation,* Academic, Newyork (1971).

28. C. de Michelis, IEEE J Quantum Electron QE-**5**, 188 (1969).

29. G. V. Ostrovskaya and A. N. Zaidel, Sov. Phys. Usp. **16**, 834 (1974).

30. C. G. Morgen, Science Prog. (LONDON) **65**, 31(1978).

31. R. G. Brewer and K. E. Riechckhoff, Phys. Rev. Lett. **13**, 334 (1964).

32. L. M. Lyamshev, Sov. Phys. Usp **24**, 977 (1981).

33. D. C. Emonny, Infrared Phys. **25**, 133 (1985).

34. N. Bolenbergen IEEE J Quantuam Electron QE-**10**, 375 (1974).

35. L. M. Lyamshev, and K. A. Naugol'nykh, Sov. Phys Acoustic **27**, 357 (1981).

36. A. C. Tam, *Ultrasensitive Laser spectroscopy,* Academic, Newyork (1983).

37. S. R. J. Brueck, H. Kildal and L. J. Belenger, Opt. Commun. **34**, 199 (1980).

38. H. M. Lie and K. Young, J Acoustic Soc. America **72**, 2000 (1982).

39. C. K. N. Patel and A. C. Tam, Rev. Mod. Phys. **53**, 517 (1981).

40. R. L. Whiteman and A, Korpel, App. Opt. **8**,1567 (1969).

41. D. A. Hutchins and F. Naduae, IEEE Ultrasonic Symposium Proceedings, IEEE Piscataway, New Jersy, p. 1175 (1983).

42. N. M. Amer, J Phys (Paris) Colloq. **C6**, 185 (1983).

43. H. Sontag and A. C. Tam, App. Phys. Lett .**46**, 725 (1985).

44. G. S. Kino, D. M. Barnet, N. Grayeli, G. Herrmann, J. V. Hunter, D. B. Ilic, G. C. Jhonson, M. P. Scott, J. C. Shyen and C. R. Steel, J. Nondestr. Eval. **1**, 67 (1980).

45. A. N. Bonderenko, B Dorbat and S. V. Kruglov, Sov .J. Nondestr. Test **12**, 665 (1976).

46. C. A. Calder and W. W. Wilcox, Mater Eval. **38**, 86 (1980).

47. I. Suemen, H. Yamamoto, and M. Yamanishi, App. Phys. Lett. **58**, 615 (1985).

48. P. Cielo, J Acoustic Soc. America suppl.1 **70**, 546 (1981).

49. R. Lucas and P. Biqard, J. Phys Radiuam. **3**, 464 (1932).

50. G. P. Davidson and D. C. Emmony, J. Phys E **13**, 92 (1980).

51. B. Sullivan and A. C. Tam, J Acoustic Soc. America **75**, 432 (1984).

52. D. Hutchins and A, Wilkins, Appl. Phys. Lett. **47**, 789 (1985).

53. C. C. William, Appl. Phys. Lett **44**, 1115 (1984).